Exploring Adipose Tissue Structure by Methylsalicylate Clearing and 3D Imaging

Jérôme Gilleron, Cindy Meziat, André Sulen, Stoyan Ivanov, Jennifer Jager, David Estève, Catherine Muller, Jean-Francois Tanti, Mireille Cormont

▶ **To cite this version:**

Jérôme Gilleron, Cindy Meziat, André Sulen, Stoyan Ivanov, Jennifer Jager, et al.. Exploring Adipose Tissue Structure by Methylsalicylate Clearing and 3D Imaging. Journal of visualized experiments : JoVE, 2020, 162, pp.e61640. ⟨10.3791/61640⟩. ⟨hal-03033057⟩

HAL Id: hal-03033057

https://hal.science/hal-03033057v1

Submitted on 14 Dec 2020

HAL is a multi-disciplinary open access archive for the deposit and dissemination of scientific research documents, whether they are published or not. The documents may come from teaching and research institutions in France or abroad, or from public or private research centers.

L'archive ouverte pluridisciplinaire **HAL**, est destinée au dépôt et à la diffusion de documents scientifiques de niveau recherche, publiés ou non, émanant des établissements d'enseignement et de recherche français ou étrangers, des laboratoires publics ou privés.

HAL Authorization

TITLE:
Exploring Adipose Tissue Structure by Methylsalicylate Clearing and 3D Imaging

AUTHORS & AFFILIATIONS:
Jérôme GILLERON[1], Cindy MEZIAT[1], André Sulen[2], Stoyan IVANOV[3], Jennifer JAGER[1], David Estève[4], Catherine Muller[4], Jean-François TANTI[1] and Mireille CORMONT[1]

[1]Université Côte d'Azur, Inserm UMR1065, C3M, Team "Cellular and Molecular Pathophysiology of Obesity", Nice, France
[2]Integrated Cardio Metabolic Center, Department of Medicine, Karolinska Institutet, Stockholm, Sweden
[3]Université Côte d'Azur, Inserm UMR1065, C3M, Team "Haematometabolism in Diseases", Nice, France
[4]Institut de Pharmacologie et de Biologie Structurale (IPBS), Université de Toulouse, CNRS, UPS, Toulouse, France

gilleron@unice.fr
Cindy.MEZIAT@univ-cotedazur.fr
Andre.Sulen@uib.no
Stoyan.IVANOV@univ-cotedazur.fr
Jennifer.JAGER@univ-cotedazur.fr
David.Esteve@ipbs.fr
Catherine.Muller@ipbs.fr
Jean-Francois.TANTI@unice.fr
Mireille.Cormont@unice.fr

Correspondence to:
Jérôme Gilleron
jerome.gilleron@univ-cotedazur.fr

KEYWORDS:
Adipose tissue, clearing, light microscopy, 3-D whole tissue, obesity, morphology.

SUMMARY:
Here, we describe a simple, inexpensive and fast clearing method to resolve the 3D structure of both mouse and human white adipose tissue using a combination of markers to visualize vasculature, nuclei, immune cells, neurons, and lipid-droplet coat proteins by fluorescent imaging.

ABSTRACT:
Obesity is a major worldwide public health issue that increases the risk to develop cardiovascular diseases, type-2 diabetes, and liver diseases. Obesity is characterized by an increase in adipose tissue (AT) mass due to adipocyte hyperplasia and/or hypertrophia, leading to profound remodeling of its three-dimensional structure. Indeed, the maximal capacity of AT

to expand during obesity is pivotal to the development of obesity-associated pathologies. This AT expansion is an important homeostatic mechanism to enable adaptation to an excess of energy intake and to avoid deleterious lipid spillover to other metabolic organs, such as muscle and liver. Therefore, understanding the structural remodeling that leads to the failure of AT expansion is a fundamental question with high clinical applicability. In this article, we describe a simple and fast clearing method that is routinely used in the laboratory to explore the morphology of mouse and human white adipose tissue by fluorescent imaging. This optimized AT clearing method is easily performed in any standard laboratory equipped with a chemical hood, a temperature-controlled orbital shaker and a fluorescent microscope. Moreover, the chemical compounds used are readily available. Importantly, this method allows one to resolve the 3D AT structure by staining various markers to specifically visualize the adipocytes, the neuronal and vascular networks, and the innate and adaptive immune cells distribution.

INTRODUCTION:

Obesity is characterized by an increase in adipose tissue mass and has become a major worldwide public health issue, given that people with obesity have increased risk of developing cardiovascular disease, type-2 diabetes, liver diseases and some cancers.

A fundamental physiological function of adipose tissue is to modulate whole-body glucose and lipid homeostasis[1,2]. During the feeding period, the adipocytes (i.e., the main cells of the adipose tissue) stores the excess glucose and lipids provided by a meal into triglycerides. During fasting, the adipocytes break down the triglycerides into non-esterified fatty acids and glycerol to sustain the energy demand of the body. During the development of obesity, adipose tissue expand by increasing the size (hypertrophia) and/or the number (hyperplasia) of adipocytes[1], to increase their storage capacity. When the expansion of adipose tissue reaches its limit, a constant highly variable among patients, the remaining lipids accumulates into other metabolic organs including muscles and liver[3,4], leading to their functional failure and initiating obesity-related cardio-metabolic complications[1,5]. Therefore, identifying the mechanisms that govern adipose tissue expansion is a key clinical challenge.

The morphological modifications documented within adipose tissues during obesity are linked to its pathological dysfunction. Several staining procedures have been used to describe the tissue organization of the adipose tissue, including actin[6], vascular markers[7], lipid-droplet markers[8], and specific immune cell markers[9,10]. However, because of the huge diameter of adipocytes (50 to 200 µm)[11], it is essential to analyze a large portion of the whole tissue in three dimensions in order to accurately analyze the dramatic structural AT changes observed during obesity. However, because the light does not penetrate an opaque tissue, imaging in 3D within a large tissue samples using fluorescence microscopy is not possible. Methods of tissue clearing to make them transparent have been reported in the literature (for a review, see[12]) allowing one to clear tissues and to perform in-depth, whole tissue fluorescence microscopy. These methods offer unprecedented opportunities to assess the 3D cellular organization in healthy and diseased tissue. Each of the described methods have advantages and drawbacks, and therefore need to be carefully selected depending on the studied tissue (for a review, see[13]). Indeed, some approaches require a long incubation period and/or the use of materials or

compounds that are either expensive, toxic or difficult to obtain[14-19]. Taking advantage of one of the first compounds used a century ago by Werner Spalteholz to clear tissues[20], we set up a user-friendly and inexpensive protocol that is very well adapted for the clearing of all mouse and human adipose tissue depots in any laboratory with typical equipment including a chemical hood, a temperature-controlled orbital shaker and a confocal microscope.

PROTOCOL:

This protocol was tested and is validated for all mouse and human white adipose tissue depots. Human and mouse adipose tissues were collected accordingly to European laws and approved by French and Swedish Ethical committees.

1. Fixation of mouse and human white adipose tissue

1.1. Immerse the harvested mouse or human white adipose tissues in at least 10 mL of PBS containing 4% paraformaldehyde (PFA) in a 15 mL plastic tube.

1.2. Shake the plastic tube at room temperature on a rolling plate for 1 h.

1.3. Leave the plastic tube at 4 °C on a rolling plate overnight, to complete the fixation.

NOTE: This protocol is adapted for large adipose tissue samples, such as whole epididymal fat pads obtained from mice fed a normal diet (≈250 mg - ≈0.6 cm^3). For larger samples like epididymal fat pads obtained from mice fed a high fat diet (≈1.5 g - ≈4 cm^3) or human adipose tissue samples, although the clearing protocol should perfectly work for the whole sample (by scaling-up the PFA and the antibody mixtures), in general, we cut tissue pieces around 1 g (≈2.5 cm^3) to reserve the remaining samples either for additional staining or applications. For the PFA (step 1.1.) we recommend using roughly 10 times the volume of the tissue. For the antibody mixtures (steps 3.1. and 3.4.), increase the volume to completely immerse the tissue, and use a 15 mL plastic tube (see **Table of Materials**) if the tissue is too large for a 1.5 mL plastic microtube (see **Table of Materials**).

2. Permeabilization and saturation of mouse and human white adipose tissue

2.1. Rinse the fixed white adipose tissue in 10 mL of PBS for 5 min at room temperature to remove all traces of PFA.

2.2. Immerse the tissue in a 15 mL plastic tube containing 10 mL of PBS supplemented with 0.3% glycine (see **Table of Materials**) and shake the tube at room temperature in an orbital shaker for 1 h at 100 revolutions per minute (rpm) to quench the remaining free aldehyde groups.

2.3. Immerse the tissue in a 15 mL plastic tube containing 10 mL of PBS supplemented with 0.2% Triton X-100 (see **Table of Materials**) and shake the tube at 37 °C in a temperature-

controlled orbital shaker for 2 h at 100 rpm.

2.4. Immerse the tissue in a 15 mL plastic tube containing 10 mL of PBS supplemented with 0.2% Triton X-100 and 20% DMSO (see **Table of Materials**) and shake the tube at 37 °C in a temperature-controlled orbital shaker at 100 rpm overnight.

2.5. Immerse the tissue in a 15 mL plastic tube containing 10 mL of PBS supplemented with 0.1% Tween-20 (see **Table of Materials**), 0.1% Triton X-100, 0.1% deoxycholate (see **Table of Materials**) and 20% DMSO and shake the tube at 37 °C in a temperature-controlled orbital shaker at 100 rpm for at least 24 h.

2.6. Rinse the tissue in a 15 mL plastic tube containing 10 mL of PBS supplemented with 0.2% Triton X-100 and shake the tube at room temperature in an orbital shaker at 100 rpm for 1 h.

2.7. Immerse the tissue in a 15 mL plastic tube containing 10 mL of PBS supplemented with 0.2% Triton X-100, 10% DMSO and 3% BSA (see **Table of Materials**) and shake the tube at 37 °C in a temperature-controlled orbital shaker at 100 rpm for 12 h, to saturate any sites that could non-specifically bind antibodies.

NOTE: In step 2.7, the BSA can be substituted by blood serum of the species of the secondary antibody used.

3. Staining procedure for mouse and human white adipose tissue

3.1. Transfer the tissue in a 1.5 mL plastic microtube containing 300 µL of PBS supplemented with 0.2% Triton X-100, 10% DMSO, 3% BSA and the primary antibodies (10x more concentrated than for cryosection staining but optimal antibody concentration should be evaluated for each antibody). Protect the tube from light by covering with aluminium foil and shake the tube at 37 °C in a temperature-controlled orbital shaker at 100 rpm for at least 2 days (see the note in step 1.1 and step 3.7.1).

3.2. Rinse the tissue in a 15 mL plastic tube containing 10 mL of PBS supplemented with 0.2% Triton X-100, 10% DMSO and 3% BSA and shake the tube protected from light at 37 °C in a temperature-controlled orbital shaker at 100 rpm for 5 h. Perform this step twice.

3.3. Rinse the tissue in a 15 mL plastic tube containing 10 mL of PBS supplemented with 0.2% Triton X-100, 10% DMSO and 3% BSA and shake the tube, protected from light, at 37 °C in a temperature-controlled orbital shaker at 100 rpm for one night to two days.

3.4. Transfer the tissue to a 1.5 mL plastic microtube containing 300 µL of PBS supplemented with 0.2% Triton X-100, 10% DMSO, 3% BSA and the secondary antibodies (10x more concentrated than for cryosection staining). Protect the tube from light by covering with aluminium foil and shake the tube at 37 °C in a temperature-controlled orbital shaker at 100 rpm for at least 2 days (see the note in step 1.1 and step 3.7.1).

3.5. Rinse the tissue in a 15 mL plastic tube containing 10 mL of PBS supplemented with 0.2% Triton X-100, 10% DMSO, and 3% BSA and shake the tube, protected from light, at 37 °C in a temperature-controlled orbital shaker at 100 rpm for 5 h. Perform this step twice.

3.6. Rinse the tissue in a 15 mL plastic tube containing 10 mL of PBS supplemented with 0.2% Triton X-100, 10% DMSO, and 3% BSA and shake the tube, protected from light, at 37 °C in a temperature-controlled orbital shaker at 100 rpm for one night to two days.

3.7. Rinse the tissue in a 15 mL plastic tube containing 10 mL of PBS and shake the tube, protected from light, at 37 °C in a temperature-controlled orbital shaker at 100 rpm for 2 h.

3.7.1. For the labelling of specific structures such as nuclei or actin, add 4',6-diamidino-2-phenylindole (DAPI or equivalent) and/or the fluorescently labelled-phalloidin at step 3.1. when only fluorescently labelled primary antibodies are used, or at step 3.4. when secondary antibodies are used.

NOTE: For the staining procedure, primary antibodies already conjugated with fluorochromes (like those used for flow cytometry) can be used and we recommend it for the gain of time and specificity. Indeed, even if mouse primary antibodies can be used followed by secondary anti-mouse antibodies, as we demonstrated it here, we have often observed non-specific staining of blood vessels due to circulating immunoglobulin. Therefore, to avoid this issue, primary antibodies that are already labelled are highly recommended and here we provide evidence that the antibodies used in flow cytometry are compatible with our procedure. However, in the specific case of an antigen that is expressed at low levels, a signal amplification step via secondary antibodies is mandatory; when the only available primary antibody is made in mouse, a cardiac-perfusion of the mice with PBS for at least 5 min at the sacrifice can remove a large proportion of circulating immunoglobulin and thus the non-specific staining.

4. Clearing procedure for mouse and human white adipose tissue

4.1. Immerse the tissue in a 15 mL plastic tube containing 10 mL of 50% ethanol and shake the tube, protected from light, at room temperature in an orbital shaker at 100 rpm for 2 h.

4.2. Immerse the tissue in a 15 mL plastic tube containing 10 mL of 70% ethanol and shake the tube, protected from light, at room temperature in an orbital shaker at 100 rpm for 2 h.

4.3. Immerse the tissue in a 15 mL plastic tube containing 10 mL of 95% ethanol and shake the tube, protected from light, at room temperature in an orbital shaker at 100 rpm for 2 h.

4.4. Immerse the tissue in a 15 mL plastic tube containing 10 mL of 100% ethanol and shake the tube, protected from light, at room temperature in an orbital shaker at 100 rpm for 2 h.

4.5. Immerse the tissue in a 15 mL plastic tube containing 10 mL of 100% ethanol and shake

the tube, protected from light, at room temperature in an orbital shaker at 100 rpm overnight.

4.6. Immerse the tissue in a 20 mL glass bottle with a plastic cap (see table of materials) containing 5 mL of methyl salicylate (see table of materials) under a chemical hood and shake the glass container, protected from light, at room temperature in an orbital shaker at 100 rpm for at least 2 h.

NOTE: The clearing procedure could be significantly accelerated (if necessary) by avoiding steps 4.3. and 4.5., although the final clearing quality would be slightly reduced.

5. 3D-confocal imaging of cleared white adipose tissue

5.1. Transfer the tissue to a metallic imaging chamber equipped with a glass bottom (see **Table of Materials**) under a chemical hood and fill the chamber with fresh methyl salicylate.

5.1.1. To secure the tissue in place, and thus to prevent it from floating or moving sideways in the chamber, apply multiple 18 mm round glass coverslips (see **Table of Materials**) on top of the tissue when mounting it into the chamber.

5.2. Place the imaging chamber on an inverted confocal microscope.

5.3. Image the tissue using a low magnification objective (e.g., 4x objective) to generate a few cm^3 3D maps of the whole adipose tissue or of the human tissue sample.

5.4. Select several areas for the tissue sampling at higher magnification. Typically, use a 20x long distance air objective that provides a good ratio between resolution and depth. We acquire large mosaic images with z-stacks between 600 and 2000 µm depth.

5.4.1. Use a long-distance objective to image deeper into the tissue.

6. Extraction of quantitative results from the 3D adipose tissue images

NOTE: The segmentation of the different structures and the subsequent extraction of the quantitative information from the 3D-image stack generated in point 5 can be performed using any of the many existing image analysis software options, either commercial or freeware. In the following points, we describe a strategy that is routinely used in our laboratory to extract quantitative information from 3D adipose tissue images using commercial software (see **Table of Materials**).

6.1. Convert the 3D stacks onto the software format to free-up memory space.

6.2. Segment the cells.

6.2.1. Open the **Cell** module of the software.

6.2.2. Change the **Cell Detection** setting to plasma membrane staining.

6.2.3. Choose the fluorescent channel of the marker used to delineate the cell periphery (phalloidin which labels cortical actin or plasma membrane markers such as F4/80 for macrophage, TCR-β for T cells, or cluster of differentiation CD proteins specific for immune cell subtypes).

6.2.4. Set up the thresholds and provide a range of expected cell size (i.e., 1 to 200 µm for cell detection).

6.2.5. Run the segmentation. A volume corresponding to the z-stack will be generated with the segmented cells color-coded with a different color for each of the neighbouring cells.

6.2.6. Apply statistical filters (size, roundness, circularity, etc.) in the statistic tab to exclude segmentation artefacts and/or to refine the segmented cells to the cell of interest based on their size (i.e., 20-200 µm for adipocytes; 5-25 µm for macrophages; 1-3 µm for lymphocytes).

6.2.7. Extract measurements and quantitative data (volume, number, size, diameter, etc.) from the statistics tab.

6.3. Segment cellular components (nuclei, vesicles, etc.) or vessels as a structure.

NOTE: Although the filament segmentation is very useful to study the connectivity of the vessels, we use the surface module segmentation to extract data on the size, volume and diameters of the vessels. Indeed, the quantification of the sizes of the vessels is lost when using the filaments module.

6.3.1. Open the **Surface** module of the software.

6.3.2. Select the fluorescent channel of the marker used to specifically label the subcellular component to reconstruct it in 3D.

6.3.3. Set up the thresholds and provide a range of the expected diameter size of the structure (i.e., 0.5-5 µm for nuclei; 0-100 µm for vessels; etc.).

6.3.4. Run the segmentation. A volume with the segmented cellular structure will be generated. Measurements and quantitative data (volume, number, size, diameter, etc.) can be extracted from the statistics tab.

6.4. Segment the vessels as a tubular continuum.

NOTE: Although the filament segmentation is very useful to study the connectivity of the vessels, we use the surface module segmentation to extract data on the size, volume and

diameters of the vessels. Indeed, the quantification of the sizes of the vessels is lost when using the filaments module.

6.4.1. Open the **Filaments** module of the software.

6.4.2. Select the fluorescent channel corresponding to the vessel staining.

6.4.3. Set up the thresholds for the fluorescence intensity and select the appropriate number of expected connecting nodes.

6.4.4. Run the segmentation. Filaments representing vessel network will be generated in 3D. Measurements can be extracted from the statistics tab, allowing to obtain quantitative data including vessel length, number of vessel branching, etc.

REPRESENTATIVE RESULTS:

Using the procedure described here and summarized in **Figure 1**, we were able to stain and optically clear human and mouse white adipose tissue as presented in **Figure 2A** and **Figure 2B,** respectively. The cleared tissue was transferred to the metallic imaging chamber to perform confocal imaging (**Figure 3A**). The clearing drastically improved the depth of the tissue images that we were able to acquire (**Figure 3B and Figure 3C).** The whole adipose tissue can be acquired in 3D at low magnification using a 4x objective (see **supplementary movie 1 and supplementary movie 2)**, to generate a 3D map, enabling to select the different areas to be acquired at high magnification using a 20x objective (**Figure 3D).** The high magnification images are acquired in 3D with a depth of 2 mm (**Figure 3E**).

This procedure enables the labelling of numerous general cell markers, including nuclei by using DAPI and actin by using fluorescently-labelled Phalloidin. Specific staining of lipid droplets and adipocytes can be achieved by using perilipin antibody (see table of materials; **Figure 4A**) and anti-Glut4 antibody (see table of materials; **Figure 4B**) respectively. Blood vessels can be detected by using either the CD31 antibody (see table of materials; **Figure 4C**) or by an intravenous injection of lectin-DyLight649 shortly prior to mouse sacrifice (see table of materials; **Figure 4D**). Macrophages and T-cells can be visualized by using the anti-CD301-PhycoErythrin antibody (see table of materials; **Figure 4D**) and the anti-TCR-β-Pacific Bleu antibody (see table of materials; **Figure 4E**). The peripheral nerve network can be detected by using the anti-Tyrosine Hydroxylase (TH) antibody (see table of materials; **Figure 4F-G**). Additionally, this protocol allows the clearing of mouse epididymal adipose tissue (**Figure 4A-B, E**), mouse subcutaneous adipose tissue (**Figure 4D, G**), mouse brown adipose tissue (**Figure 4F**), and human adipose tissue (**Figure 4C**). Using a combination of these labelling and a commercial software (see table of materials) to segment these markers, we can determine within the adipose tissue i) adipocytes mean size and size distribution (**Figure 5A-B**) and ii) blood vessel network density (**Figure 5C**).

FIGURE LEGENDS:

Figure 1. **Summary of the clearing procedure for white adipose tissue.** Mouse or human white

adipose tissues are fixed, permeabilized, saturated, stained and cleared. Images are then acquired in 3D and analyzed using a commercial software.

Figure 2. Photographs of white adipose tissue. (A) Photograph of human white abdominopelvic adipose tissue before and after the clearing procedure. **(B)** Photograph of mouse epididymal white adipose tissue before and after the clearing procedure.

Figure 3. Improved imaging depth with adipose tissue clearing. (A) Mounting of the metallic imaging chamber equipped with glass bottom. **(B)** Z-series images of mouse epididymal white adipose tissue stained with phalloidin-Alexa488 (green) before and after clearing. **(C)** XZ projections corresponding to the white dotted lines across the panel B z-stack. **(D)** Z-projection of 0.4 cm z-stack of mouse subcutaneous white adipose tissue stained for actin using Phalloidin-Alexa488 and acquired at low magnification with a 4x objective. The small images on the right were acquired at the selected tissue position using a 20x objective. **(E)** Side view of the 3D volume rendering of image z-stack from cleared mouse white adipose tissue stained with Phalloidin-Alexa488 acquired similarly to the 20x images from **(D)**. The 3D imaging depth achieved by our high magnification procedure is demonstrated here and underlined by a z-depth color coding (dark blue for z=0 mm to dark red for z=2 mm).

Figure 4. Mouse and human white adipose tissues stained for several markers. (A) Single plane image of mouse epididymal white adipose tissue stained for lipid droplets using anti-perilipin1 antibody and anti-mouse-alexa647-conjugated antibody. **(B)** Mosaic single plane image of mouse epididymal white adipose tissue stained for nuclei and adipocytes using DAPI, anti-Glut4 antibody and anti-mouse-alexa647-conjugated antibody. **(C)** Z-projection of 600 µm z-stack of human white abdominopelvic adipose tissue stained for vessels using CD31-alexa647-conjugated antibody. **(D)** Z-projection of 600 µm z-stack of mouse subcutaneous white adipose tissue stained for vessels and macrophages using lectin-DyLight649 intravenous injections and anti-CD301-alexa555 antibody. The lower right inset is a zoomed image of the white dotted box. **(E)** Single plane image of mouse epididymal white adipose tissue stained for actin and T-cells using phalloidin-Alexa488 and anti-TCRβ-Pacific blue-conjugated. The lower right inset is a zoomed image of the white dotted box. **(F)** Z-projection of 50 µm z-stack of mouse brown adipose tissue stained for nuclei and neuronal network using DAPI, anti-TH antibody and anti-rabbit-alexa647-conjugated antibody. **(G)** Z-projection of 600 µm z-stack of mouse subcutaneous white adipose tissue stained for nuclei and neuronal network using DAPI, anti-TH antibody and anti-rabbit-alexa647-conjugated antibody.

Figure 5. Analysis of 3D images using commercially available software (see table of materials)**. (A)** 3D volume rendering of human adipocytes segmented in 3D by commercially available software. Every adipocyte has a different color to its contacting adjacent adipocytes. Vessels are represented in red. **(B)** Size quantification and distribution of the adipocytes from the 3D volume rendering of panel A, which contains around 20,000 adipocytes. **(C)** 3D volume rendering of blood vessels segmented in 3D using commercially available software and represented in red or yellow for the large and small vessels, respectively.

Supplementary Movie 1. 3D volume rendering of the whole subcutaneous white adipose tissue shown in Figure 3D. The white box represents a 2 cm^3 cube.

DISCUSSION:

The modifications that occur within the adipose tissue over the course of pathological progression, such as that of obesity, is fundamental to the understanding of the mechanisms behind the pathology. Pioneering studies that revealed such mechanisms in adipose tissue have been based on global approaches such as whole adipose tissue proteomics[21], flow cytometry[22,23], and transcriptomics[24,25]. In addition, efforts have been made to explore the structural changes occurring in adipose tissue using histological analyses[26-29]. However, the analysis of 5-10 µm adipose tissue sections, because of the limited size of the section, restricts the ability to appreciate important structural features. First, only a few adipocyte nuclei are detectable per section since each section represents only a small portion of the adipocytes ($1/10^{th}$). Second, the size of the adipocytes estimated from adipose tissue sections is inaccurate because most adipocytes are cut below or behind their equator, leading to a biased (under)measurement of their mean size. Third, the blood vessel and nerve fiber continuum are lost during physical sectioning. Fourth, the distribution of each subtypes of immune cells within the tissue is difficult to establish because the three-dimensional coordinates are lost. In this context, the methodology we propose here allows any standard laboratory to image human and mouse white adipose tissue in three-dimensions, in a simple and inexpensive manner.

This method does have some limitations. First, the time required to prepare the tissue (fixation, permeabilization, staining, clearing) is long (more than a week). This would be difficult to reduce because the majority of this time is required to stain the tissue. The penetration of antibodies within such large tissue samples requires long incubation times. Decreasing the incubation time would increase the risk of having non-homogenous antibody penetration, which would lead to staining artifacts. Therefore, the only possible window to gain time and shorten the procedure is the time dedicated to clear the tissue, which takes around one day when optimal results are required, but this can be decreased to half a day without a dramatic drop in quality. The second limitation is the probable shrinkage of the tissue. Indeed, in any protocol that dehydrates tissue using solvents, it is likely that the tissues shrink due to water removal. Estimating this shrinkage is always challenging, and it is nearly impossible here because the edge of the tissue becomes transparent when lipids start to be extracted during the dehydration process. Hence, the size estimations of the cleared tissues need to be interpreted with caution. However, comparing changes in adipocyte sizes or vessel length between tissues derived from mouse with different genotypes and/or submitted to different environmental conditions remain informative[11]. The last limitation is linked to the large volume of the whole mouse adipose tissue or of a large human adipose tissue surgical sample. Indeed, although the protocol is perfectly adapted to clear these large samples, imaging a whole organ is challenging with a confocal microscope. The strategy to overcome this issue and to exploit the full potential of the whole organ clearing procedure, is to acquire a 3D low magnification map of the whole organ by using a 4x objective, and to select specific areas randomly dispersed within the tissue where higher magnification 3D images using a 20x long-distance objective can be acquired. The “high magnification” setup allows imaging the tissue volume of around 45

mm^3 (4.7 x 4.7 x 2 mm). Although this volume is limited compared to the volume of the whole organ (0.5 to more than $4cm^3$), repeating the acquisitions at several positions within the tissue allows us to obtain a good sampling of the tissue at cellular to sub-cellular resolution. Note that imaging large tissues will generate a significant amount of imaging data that will need to be stored.

The procedure has significant differences when compared to methods that have previously been described to clear adipose tissue[14,30]. First of all, unlike AdipoClear, that uses methanol, dichloromethane, and dibenzylether[14], the method presented here uses ethanol for dehydration and methyl salicylate for clearing. Therefore, the procedure is safer because it takes advantage of less toxic clearing solvents that are often used by food/drink-processing industries (ethanol and methylsalicylate), in comparison to the high toxicity of dichloromethane, methanol and dibenzylether. Moreover, the preparation of the tissue according to the protocol is two days faster than the AdipoClear protocol[14]. More recently, another method was proposed by Li and colleagues to clear adipose tissue pieces by immersing them into glycerol[30]. This protocol is very simple even compared to thid procedure, and the quality of the images is good even at high magnification. However, this clearing protocol only works efficiently when using 2 mm^3 adipose tissue pieces. The sectioning of the tissue into these tiny samples prior to the clearing procedure prevents one from imaging tissue volumes larger than 2 mm^3 even at low magnification. The procedure presented here allows mapping of the whole tissue in 3D at low magnification and acquisition of 3D stacks of images around 45 mm^3 at several known positions within the whole cleared adipose tissue at high magnification.

This procedure may have several future applications. As with any method, the procedure described here can be simplified and/or further optimized. An interesting advance for the procedure could come from the combination of the clearing process, we described, with additional imaging approaches. For example, specific imaging setups, such as Optical Projection Tomography (OPT), Total Internal Reflection Fluorescence microscopy (TIRF), Selective Plan Illumination Microscopy (SPIM) or Stimulated Emission Depletion microscopy (STED) are in principle compatible with the procedure, although this will limit its applicability to those laboratories that are equipped with these systems. Alternatively, using an objective with a high numerical aperture index and an acquisition system that is able to acquire hundreds of images per second, which is found in many laboratories, one could perform super-resolution analyses by using the Super Resolution Radial Fluctuations (SRRF) post-processing image analysis freeware[31]. Interestingly, classical fluorochromes are adapted for the SRRF analysis, which would enable 3D super-resolution analyses of whole human and mouse white adipose tissues.

Many critical steps in the protocol are related to the tissue processing prior to the clearing itself. First of all, and as for classical histological analyses, the fixation step is fundamental. In the case of weak fixation, structural features are not preserved, whereas extended fixation leads to crosslinking and blocking of specific antigen sites and consequent non-homogeneous immuno-staining. Another sensitive step is the staining of the tissue, which presents several critical points that we will describe below. First, the antibodies need to be validated by testing them on cryostat sections to confirm that they are functional and to determine their optimal

concentration. The final concentration that is used for the clearing procedure is ten times the optimal concentration for the cryostat sections. Second, the time of incubation is also critical because of the size of the tissue. An incubation time that is too short will produce weak or non-homogeneous immunostaining (e.g., correct staining on the periphery of the tissue but no internal staining). Similarly, washing steps that are too short will prevent non-specifically-bound antibodies from being removed from the tissue leading to non-specific staining. To our knowledge, extended incubation of the tissue with antibodies does not impair the staining. Therefore, we strongly recommend long incubation and washing periods. Third, the choice of the fluorochrome must be adapted to the signal of interest. In tissue samples in general, and especially white adipose tissue, non-negligible auto-fluorescence is detectable at 488 nm and 555 nm. For highly expressed proteins this is not an issue and the staining will work well in these channels. However, for proteins with low expression we strongly recommend the use of far-red fluorochromes. For the clearing, there are no critical steps since the methodology is very simple. Keep in mind that methyl salicylate is not compatible with plastic materials, therefore we recommend glass bottles for the clearing steps and a metallic chamber equipped with a glass bottom to perform the imaging. Alternatives for this mounting procedure exist using i) a normal glass slide, dental resin and glass coverslip (to generate a small glass chamber), or ii) a glass petri-dish (for upright microscope setups).

ACKNOWLEDGMENTS:
This work was supported by INSERM, Université Côte d'Azur, and by grants from the French National Research Agency (ANR) through the Investments for the Future Labex SIGNALIFE (ANR-11-LABX-0028-01), the program UCA JEDI (ANR-15-IDEX-01) via Academy 2 "Systèmes Complexes" and Academy 4 "Complexité et diversité du vivant", and the Young Investigator Program to J.G. (ANR18-CE14-0035-01-GILLERON). We also thank the Imaging Core Facility of C3M funded by the Conseil Départemental des Alpes-Maritimes and the Région PACA, and which is also supported by the IBISA Microscopy and Imaging Platform Côte d'Azur (MICA). We thank Marion Dussot for technical help in tissue preparation. We thank Abby Cuttriss, UCA International Scientific Visibility, for proof reading of the manuscript.

DISCLOSURES:
The authors have no conflicts to disclose.

REFERENCES:
1 Pellegrinelli, V., Carobbio, S., Vidal-Puig, A. Adipose tissue plasticity: how fat depots respond differently to pathophysiological cues. *Diabetologia*. **59** (6), 1075-1088 (2016).
2 Stern, J. H., Rutkowski, J. M., Scherer, P. E. Adiponectin, Leptin, and Fatty Acids in the Maintenance of Metabolic Homeostasis through Adipose Tissue Crosstalk. *Cell Metabolism*. 23 (5), 770-784 (2016).
3 Mittendorfer, B. Origins of metabolic complications in obesity: adipose tissue and free fatty acid trafficking. *Current Opinion in Clinical Nutrition & Metabolic Care*. **14** (6), 535-541 (2011).
4 Hammarstedt, A., Gogg, S., Hedjazifar, S., Nerstedt, A., Smith, U. Impaired Adipogenesis and Dysfunctional Adipose Tissue in Human Hypertrophic Obesity. *Physiological Reviews*. **98** (4),

1911-1941 (2018).
5 Moreno-Indias, I., Tinahones, F. J. Impaired adipose tissue expandability and lipogenic capacities as ones of the main causes of metabolic disorders. *Journal of Diabetes Research*. **2015**, 970375 (2015).
6 Vergoni, B. et al. DNA Damage and the Activation of the p53 Pathway Mediate Alterations in Metabolic and Secretory Functions of Adipocytes. *Diabetes*. **65** (10), 3062-3074 (2016).
7 Xue, Y., Xu, X., Zhang, X. Q., Farokhzad, O. C., Langer, R. Preventing diet-induced obesity in mice by adipose tissue transformation and angiogenesis using targeted nanoparticles. *Proceedings of the National Academy of Sciences U S A*. **113** (20), 5552-5557 (2016).
8 Zwick, R. K. et al. Adipocyte hypertrophy and lipid dynamics underlie mammary gland remodeling after lactation. *Nature Communication*. **9** (1), 3592 (2018).
9 Zhang, L. et al. The inflammatory changes of adipose tissue in late pregnant mice. *Journal of Molecular Endocrinology*. **47** (2), 157-165 (2011).
10 Yang, H. et al. Obesity increases the production of proinflammatory mediators from adipose tissue T cells and compromises TCR repertoire diversity: implications for systemic inflammation and insulin resistance. *Journal of Immunology*. **185** (3), 1836-1845 (2010).
11 Laforest, S. et al. Comparative analysis of three human adipocyte size measurement methods and their relevance for cardiometabolic risk. *Obesity (Silver Spring)*. **25** (1), 122-131 (2017).
12 Azaripour, A. et al. A survey of clearing techniques for 3D imaging of tissues with special reference to connective tissue. *Progress in Histochemistry and Cytochemistry*. **51** (2), 9-23 (2016).
13 Richardson, D. S., Lichtman, J. W. Clarifying Tissue Clearing. *Cell*. **162** (2), 246-257 (2015).
14 Chi, J., Crane, A., Wu, Z., Cohen, P. Adipo-Clear: A Tissue Clearing Method for Three-Dimensional Imaging of Adipose Tissue. *Journal of Visualized Experiments*. 10.3791/58271 (137) (2018).
15 Roberts, D. G., Johnsonbaugh, H. B., Spence, R. D., MacKenzie-Graham, A. Optical Clearing of the Mouse Central Nervous System Using Passive CLARITY. *Journal of Visualized Experiments*. 10.3791/54025 (112) (2016).
16 Woo, J., Lee, M., Seo, J. M., Park, H. S., Cho, Y. E. Optimization of the optical transparency of rodent tissues by modified PACT-based passive clearing. *Experimental & Molecular Medicine*. **48** (12), e274 (2016).
17 Zhang, Y. et al. 3D imaging of optically cleared tissue using a simplified CLARITY method and on-chip microscopy. *Science Advances*. **3** (8), e1700553 (2017).
18 Ke, M. T., Imai, T. Optical clearing of fixed brain samples using SeeDB. *Current Protocols in Neuroscience*. **66**, Unit 2 22 (2014).
19 Hahn, C. et al. High-resolution imaging of fluorescent whole mouse brains using stabilised organic media (sDISCO). *Journal of Biophotonics*. **12** (8), e201800368 (2019).
20 Spalteholz, W. Über das Durchsichtigmachen von Menchlichen und Tierichen Präparaten und Seine Theoretischen Bedingungen. S. Hirzel, Leipzig. (1911).
21 Shields, K. J., Wu, C. Differential Adipose Tissue Proteomics. *Methods in Molecular Biology*. **1788**, 243-250 (2018).
22 Bourlier, V. et al. Remodeling phenotype of human subcutaneous adipose tissue

macrophages. *Circulation*. **117** (6), 806-815 (2008).
23 Hagberg, C. E. et al. Flow Cytometry of Mouse and Human Adipocytes for the Analysis of Browning and Cellular Heterogeneity. *Cell Reports*. **24** (10), 2746-2756 e2745 (2018).
24 Hill, D. A. et al. Distinct macrophage populations direct inflammatory versus physiological changes in adipose tissue. *Proceedings of the National Academy of Sciences U S A*. **115** (22), E5096-E5105 (2018).
25 Acosta, J. R. et al. Single cell transcriptomics suggest that human adipocyte progenitor cells constitute a homogeneous cell population. *Stem Cell Research & Therapy*. **8** (1), 250 (2017).
26 Coppack, S. W. Adipose tissue changes in obesity. *Biochemical Society Transactions*. **33** (Pt 5), 1049-1052 (2005).
27 Cancello, R. et al. Reduction of macrophage infiltration and chemoattractant gene expression changes in white adipose tissue of morbidly obese subjects after surgery-induced weight loss. *Diabetes*. **54** (8), 2277-2286 (2005).
28 Cinti, S. Adipocyte differentiation and transdifferentiation: plasticity of the adipose organ. *Journal of Endocrinology Investigation*. **25** (10), 823-835 (2002).
29 Wellen, K. E., Hotamisligil, G. S. Obesity-induced inflammatory changes in adipose tissue. *Journal of Clinical Investigation*. **112** (12), 1785-1788 (2003).
30 Li, X., Mao, Z., Yang, L., Sun, K. Co-staining Blood Vessels and Nerve Fibers in Adipose Tissue. *Journal of Visualized Experiments*. 10.3791/59266 (144) (2019).
31 Gustafsson, N. et al. Fast live-cell conventional fluorophore nanoscopy with ImageJ through super-resolution radial fluctuations. *Nature Communication*. **7**, 12471 (2016).

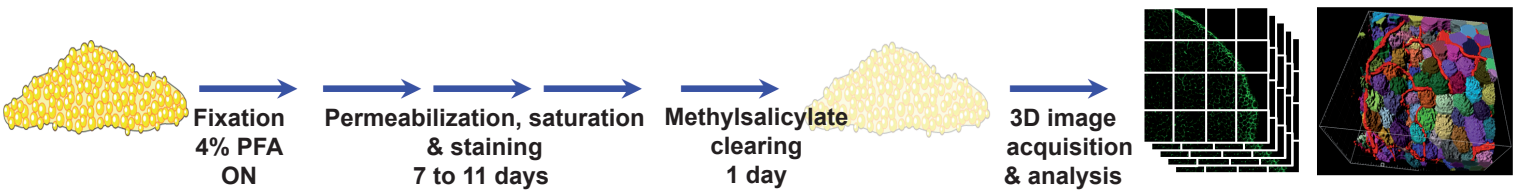
Fixation
4% PFA
ON
Permeabilization, saturation
& staining
7 to 11 days
Methylsalicylate
clearing
1 day
3D image
acquisition
& analysis

Figure 1

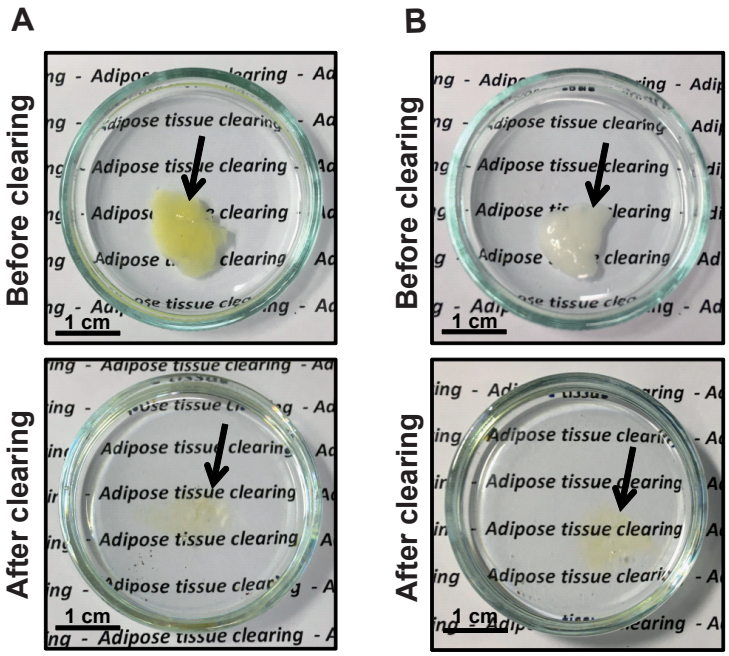
A
B
Before clearing
After clearing
1 cm
Adipose tissue clearing

Figure 2

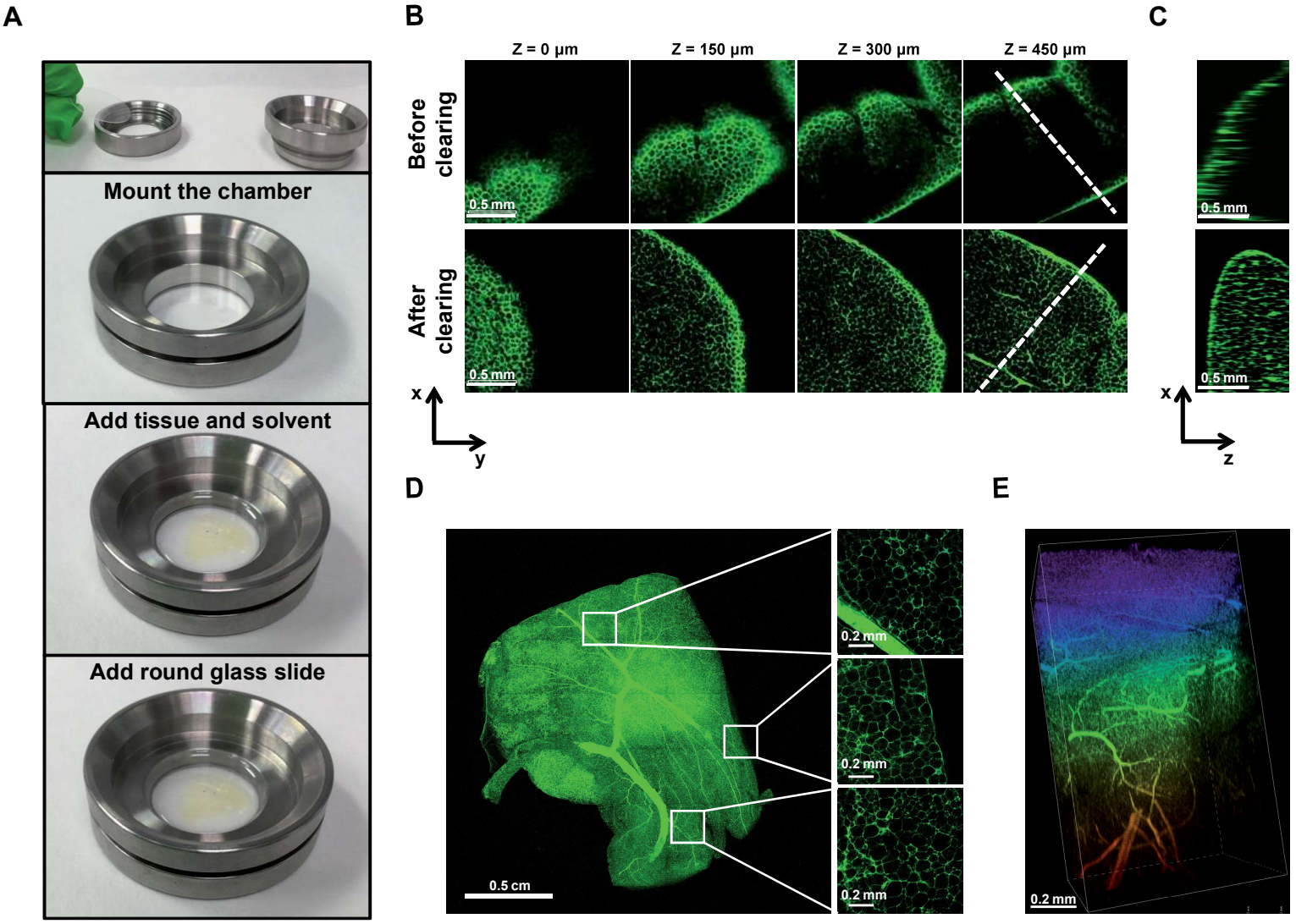
A
Mount the chamber
Add tissue and solvent
Add round glass slide
B
Z = 0 µm
Z = 150 µm
Z = 300 µm
Z = 450 µm
Before clearing
After clearing
0.5 mm
x
y
C
0.5 mm
x
z
D
0.2 mm
0.5 cm
E
0.2 mm

Figure 3

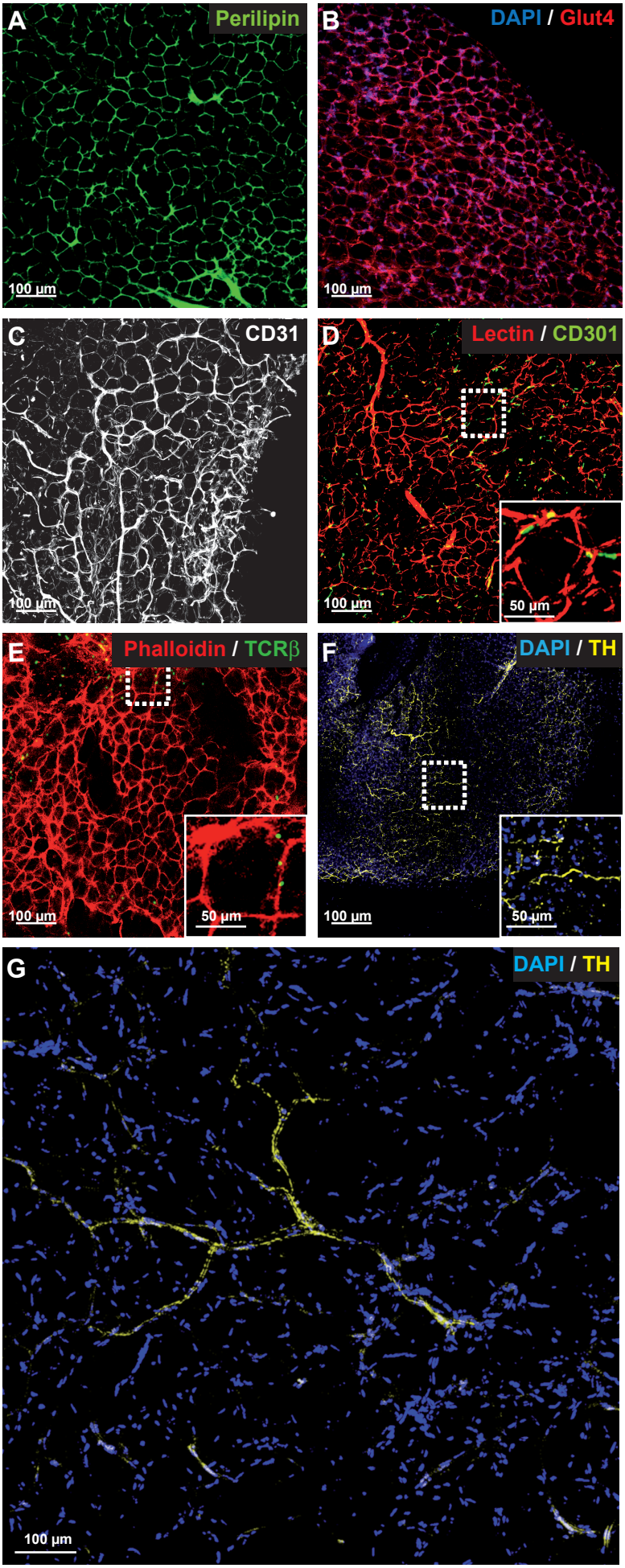
A
Perilipin
100 μm
B
DAPI / Glut4
100 μm
C
CD31
100 μm
D
Lectin / CD301
100 μm
50 μm
E
Phalloidin / TCRβ
100 μm
50 μm
F
DAPI / TH
100 μm
50 μm
G
DAPI / TH
100 μm

Figure 4

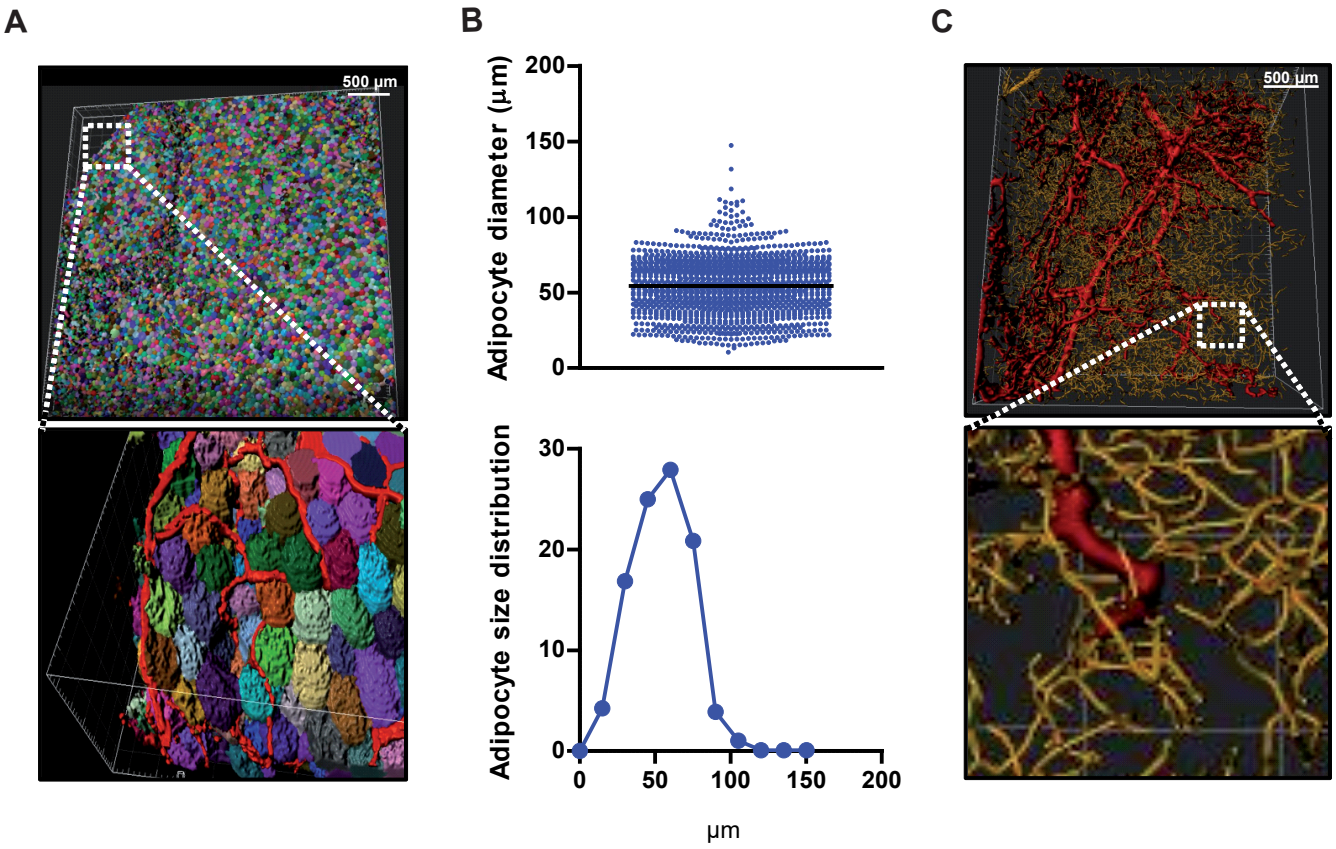
A
500 µm
B
Adipocyte diameter (µm)
200
150
100
50
0
Adipocyte size distribution
30
20
10
0
0
50
100
150
200
µm
C
500 µm

Figure 5